LA-UR-21-30045
Approved for public release; distribution is unlimited.

Title: Experimental Assessment of Elastic Modulus vs. Relative Density for Stretch- and Bend-Dominated Lattices

Author(s): Husmann, Katheryn Noel
Martinez, Elizabeth
Arinder, Graham Burton
Marchi, Alexandria Nicole

Intended for: Report

Issued: 2021-10-11

Experimental Assessment of Elastic Modulus vs. Relative Density for Stretch- and Bend-Dominated Lattices

Katheryn Husmann[a,*], Elizabeth Martinez [b], Graham Arinder[b], Alexandria N. Marchi[a]

[a]MPA-11, [b]E-1, *khusmann@lanl.gov

July 9, 2021

Table of Contents

Abstract

This project was designed to study the possibility of using structural properties of lattices to replicate the material properties of certain hard to manufacture designs and use topology optimization to determine the lattice type and density required to mimic these properties. The integration of additively manufactured lattice structures with topology optimization highlights the need for well characterized mechanical properties and uncertainty analyses to insure these optimized structures respond as predicted. Stereolithographically printed octet and rhombic dodecahedron lattices were manufactured at 10%, 25% and 65% density by volume. As a separate task, yet integrated into this work, finite element analysis (FEA) was used to predict the printed lattice's mechanical properties, which were then compared to our experimental results. After comparing FEA and experimentally-measured elastic moduli, it was determined that the FEA provides highly reliable predictions for the modulus of these printed lattice structures. These lattices also exhibited greater tensile stiffness than that of the solid material demonstrating the flexibility that lattices provide to designing parts with designer structural properties. The accurate printing and reliable modeling of these lattices will enable topology optimization of complex parts from well-characterized rhombic dodecahedron and octet lattice structures of varying densities.

Background and Research Objectives

Lattice Structures Produced/Hypothesized in the Literature

When referring to lattice structures, the material properties are the apparent macroscopic properties of structures that converge to certain values when the number of the unit cells is large enough. [1] Properties such as elastic modulus (E), ultimate strength, and toughness are the most commonly measured and compared to the properties of the solid material through testing. Many studies have completed compression testing ([1][2] [3] [4] [5]) and some have continued onto shear and bending tests. [3] The tests used to determine the macroscopic properties depend greatly on the different lattices tested as well as the 3D printing method used for manufacturing the test specimens. These lattices are designed using CAD programs like SoidWorks [5] and printed. More research is available [6].

Finite Element Analysis (FEA) is among the many types of modeling developed and used to predict the lattice material properties. Mark C. Messner has developed dynamic equivalent continuum model and later the inverse homogenization approach for optimizing the periodic structure of lattice materials, but also includes FEA as a modeling technique. [7] Messner also mentions that the lattice type influences the time and resources required to accurately model the properties. Correlations were identified between the relative density and mechanical properties of many unit cell topologies consistent with the predictions of the Gibson-Ashby model. [1] The relative density is dependent on the strut size and lattice type with most common lattice type studied is the Octet-truss. Other lattices include the iso-truss [8], a Simple beam lattice cell with diagonal beams, Schwarz's P cell, [9] BCC-Z structure, circumferential rectangular pattern of 4 vertical struts, and BCC unit cell without the vertical strut [3]. Some lattices are simply too difficult to print due to their geometries but have been optimized for the minimum surface [1] and therefore minimum density required.

Additive Manufacturing of Lattice Structures

There are many different ways to additively manufacture lattice structures including filament extrusion (FDM/FFF), binder jetting, Selective Laser Sintering/Melting (SLS/M), and Stereolithography (SLA). [1] [2] [3] [4] Filament extrusion-based lattice structures amplify the poor layer bonding and high directionality inherent in the printing process while lattices made from binder jet technologies have issues with lack of parallelism and overprinting. [5] SLS lattices display significantly differing mechanical properties from bulk because of the rapid solidification of the layers during laser printing, which are responsible for the development of non-equilibrium phases where micro segregation of chemical composition and directional grain growth may be present.[5] SLS also has many geometric defects that can be caused by a variety of issues such as suboptimal processing parameters or internal defects due to incomplete filling by the laser trajectory. Limitations of the SLS process can lead to discrepancies between the intended and as-fabricated lattice structure geometries. These discrepancies may be due to shrinkage after melting, attachment of unmelted particles or waviness and roughness of struts. SLA has freedom around printing lattice structures and material type flexibility while refraining from anisotropy due to directionality of the print. The layers bond together nearly isotropically, curing one layer onto another. SLA is accurate at printing lattices ensuring there are fewer filled voids due to over curing as long as the lattice density allows the uncured resin to have an exit path. Each of these printing methods has its applications; for these experiments, SLA was utilized.

Experimental

Stereolithography Printed Specimens

Lattices were printed using Formlabs Form 3 printers in clear V4 resin designed by Formlabs for their specific printers. Three samples of each density and type were printed (e.g. 10% 0ctet) for tension and compression testing. Each samples was cleaned thoroughly using isopropyl alcohol (IPA) and dried with nitrogen resulting in as few inclusions as possible. Each sample was then post-print cured inside a 405nm LED cure chamber heated to 60℃ for 30 minutes. After curing each sample was tested nondestructively a minimum of five times to obtain effective modulus for the lattice.

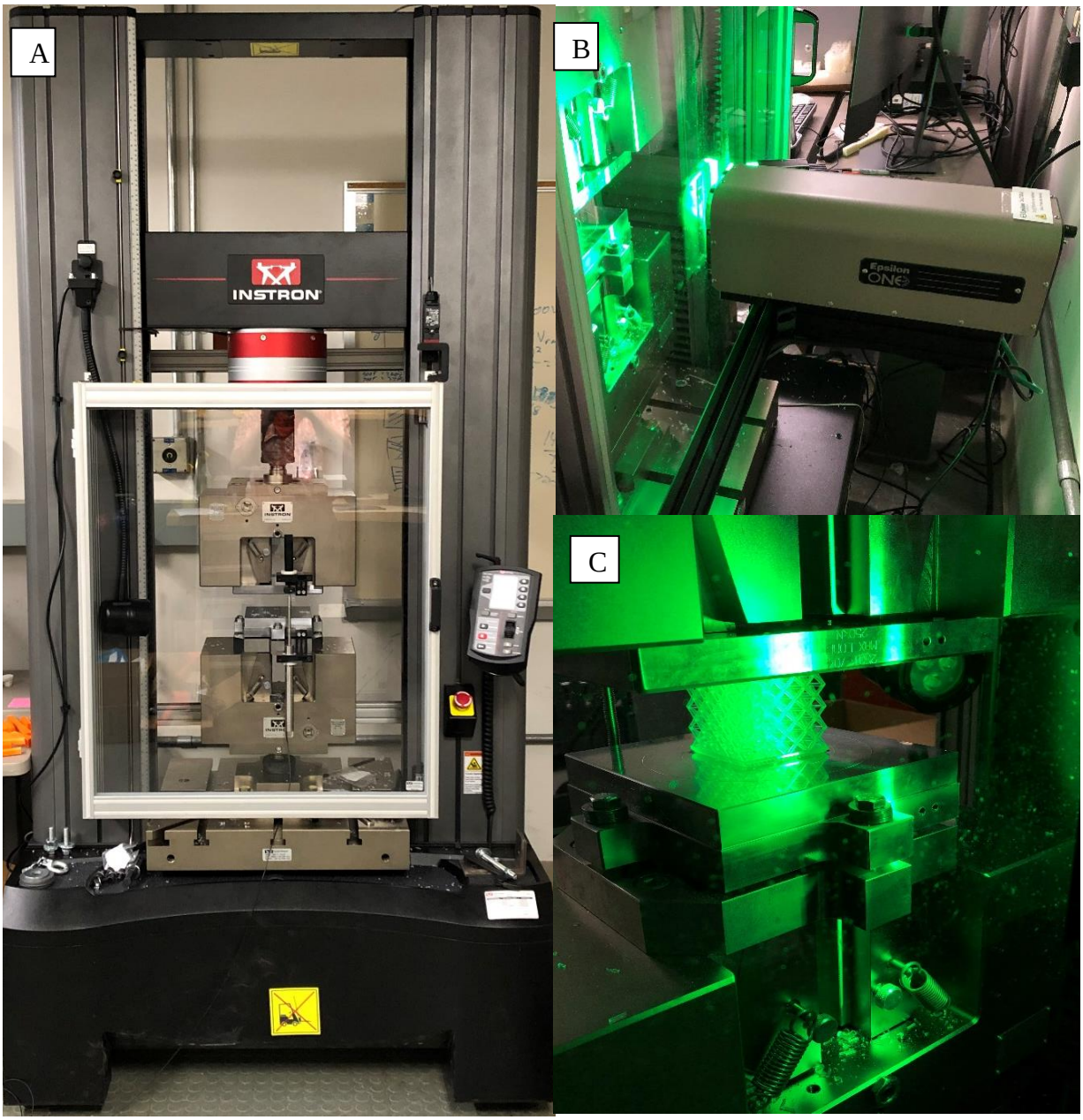

Figure 1: Photos of testing setup. 1A is of the testing set up while 1B is of the noncontact extensometer. 1C is while testing a compression samples.

Mechanical testing

Compression and tension testing was completed on an Instron 5985 dual column test frame with a 250kN load cell. The Instron data was collected and run by Blue Hill Universal software. The compression strain tests were measured by an Instron LVDT, which is a class D extensometer with a +-50mm range. The tension tested was measured by Epsilon ONE 78-PT Class B-1 non-

contact extensometer with a 50mm gauge length. The extensometers were calibrated in accordance with ASTM E-83 standard. The tests were completed following ASTM D1621 for compression with displacement rate controlled at 0.001 mm/min. Tensile tests were completed using a similar test method as compression with a custom coupon design for the experiment. Data was taken using the Epsilon One set up shown in Figure 1. Data collected from this experiment was compared to FEA modeling completed using Abaqus standard. A single layer of the lattice geometry was modeled from tensile and compression testing specimen designs. [10] The samples were designed according to figure 2.

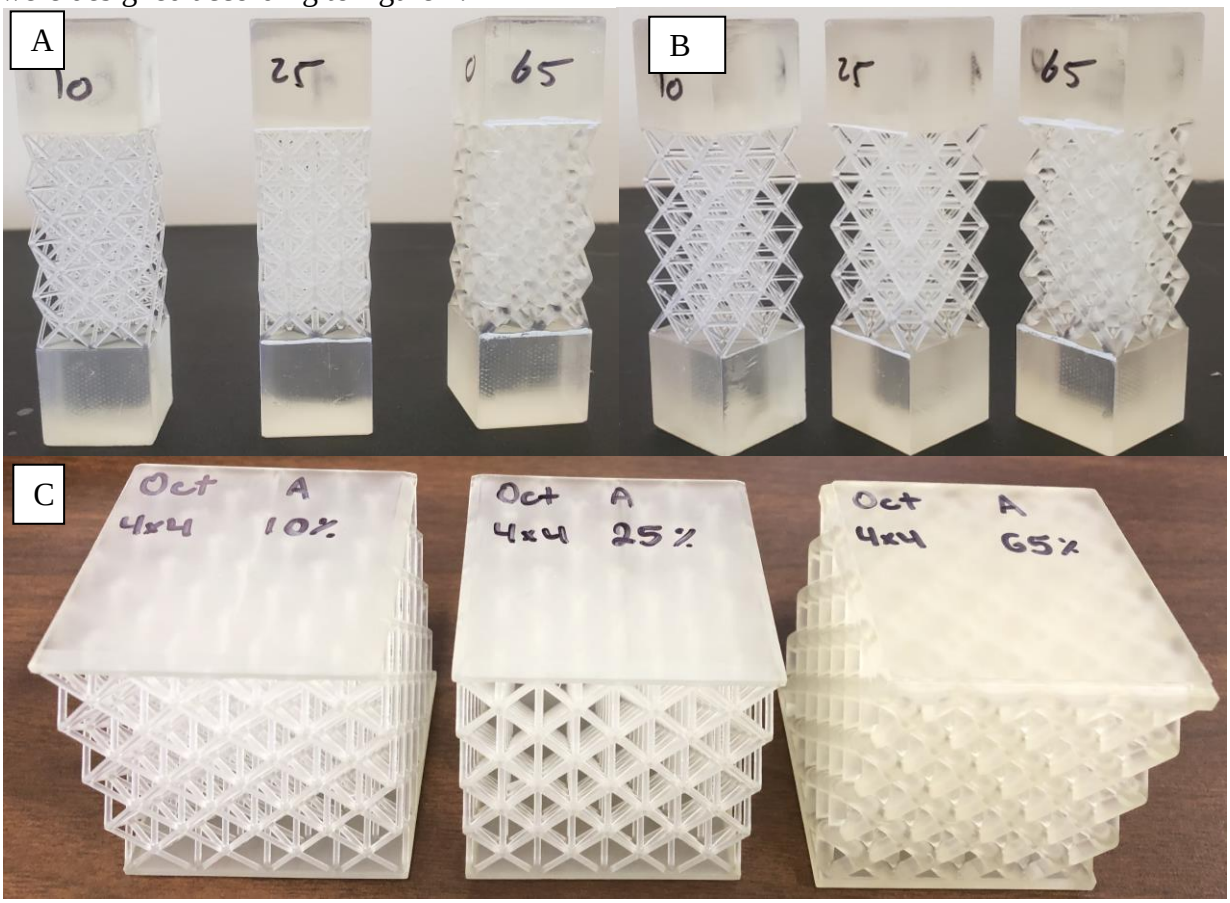

Figure 2a and 2b are of some tensile samples while Figure 2c is of some compression samples.

Data Analysis

Data analysis code was written in MATLAB in order to analyze the data gathered from the LVDT and non-contact extensometer. The code took the force and displacement data from the extensometers and used the sample cross sectional area and initial gauge length to obtain a stress vs strain curve. Each curve was numerically zeroed in order to reduce pre-test noise. Since the test was stopped well within the elastic region, the entirety of the curve was subjected to a line of best fit to determine the modulus. The modulus was tabulated and averaged when the testing for a specific lattice type and density was completed. The range and standard deviation were also calculated at this time. The average modulus for the set of curves was compared to the individual curves and a

representative curve with the closest modulus to the average was chosen for the comparative graphs. The average curve was then compared to the FEA model to determine the accuracy.

Results

Lattice Print Characterization

Prior to any mechanical testing some of the printed samples at each of the three densities, 10% 25% and 65%, were weighed for print accuracy and repeatability. The as designed densities were calculated from the as designed volumes (as calculated in the computer aided design software, SOLIDWORKS) and as designed strut diameters were compared to printed structures. The printed strut diameters were measured using calipers precise to 0.001 in while the densities were also calculated using the masses of representative printed samples measured on a high-precision scale precise to 0.0001g. Table 1 shows the uncertainty between the design and the printing method for each lattice style and density design (3 example prints per design). The print repeatability is a measure of how repeatable the printing method created the printed lattice structures. Print repeatability is calculated by finding the maximum range of the printed densities. The average print difference from as designed is an indication of how well the printed part matches the design. This is calculated as the percent difference between the average print density and the as designed density.

Table 1: table showing as designed and printed densities. Solid material density is 1.156 g/mL

Name	As Designed Density	As Designed Mass (g)	Printed Mass (g)	Printed Density	Print Repeatability	% Difference between Avg Print and As Designed Densities
Octet A	10%	35.373	38.316	10.83%	+/-0.50%	10.53%
Octet B			40.871	11.55%		
Octet C			38.106	10.77%		
RD A	10%	32.07	34.087	10.72%	+/-0.79%	15.10%
RD B			35.680	11.82%		
RD C			35.912	11.99%		
Octet A	25%	58.844	59.750	28.50%	+/-0.22%	13.92%
Octet B			60.019	28.68%		
Octet C			59.414	28.26%		
RD A	25%	53.84	53.493	24.16%	+/-0.08%	-3.11%
RD B			53.554	24.21%		
RD C			53.691	24.30%		
Octet A	65%	118.124	124.59	73.41%	+/-0.34%	13.43%
Octet B			125.00	73.70%		
Octet C			125.54	74.07%		
RD A	65%	114.97	119.63	69.97%	+/-0.87%	8.98%
RD B			121.12	71.01%		
RD C			121.87	71.53%		

Uncertainties in the density might be caused by over curing on the nodes of the lattice. The printed lattice strut diameter was between nominal and -0.004 in of the modeling diameter while the lattice density by weight measurement was on average +3.83% larger than designed. Since the 65% has the largest nodes, the most over curing occurred on 65%. The 25% and the 10% of both unit cells have masses that match the design mass within 5%, and the 65% density was within 10%.

Tensile Testing

The modulus was determined by graphing the stress vs strain data results and using linear best fit to determine the slope of this line. The mean moduli for each lattice type and density was calculated by adding all of the slopes of that type and density together and dividing by the number of samples measured. The standard deviation was taken using the root mean squared method of the moduli used for the means. Figure 3 and 4 show all of the tests compared to a printed solid sample the same dimensions as the other tests for tension and compression. Figure 5 shows all of the predicted and tested moduli. The tested moduli shown in Figure 5 are the mean modulus for that type and density.

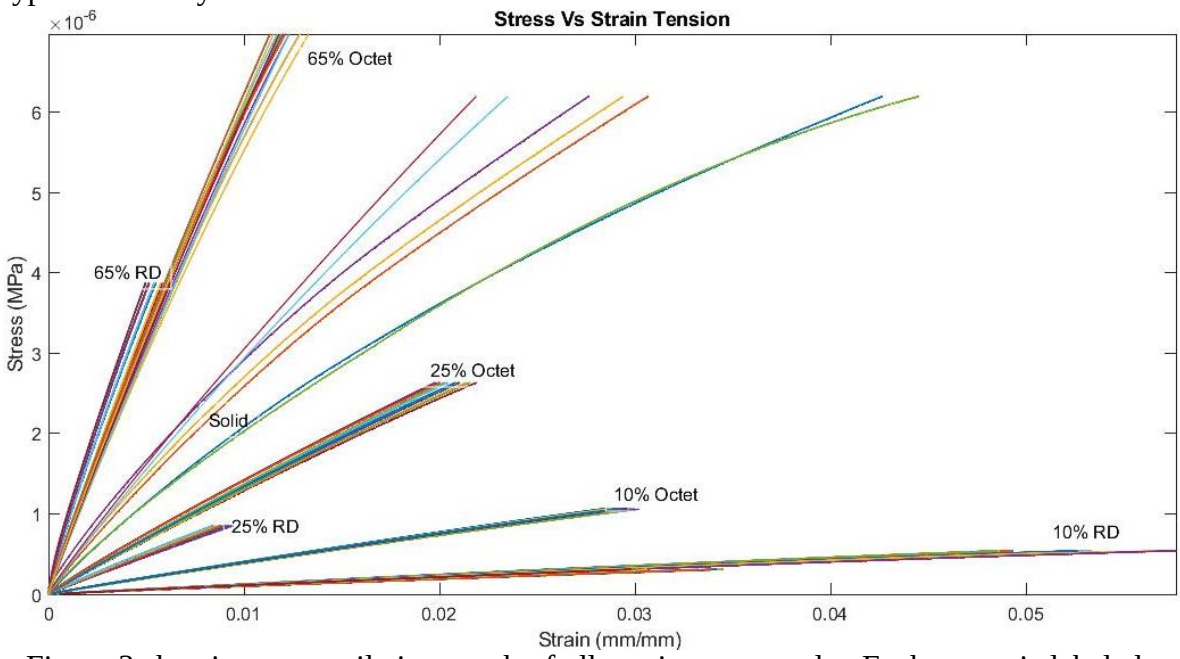

Figure 3 showing a compilation graph of all tension test results. Each group is labeled on the graph as to the type and density with which it corresponds.

Compression Testing

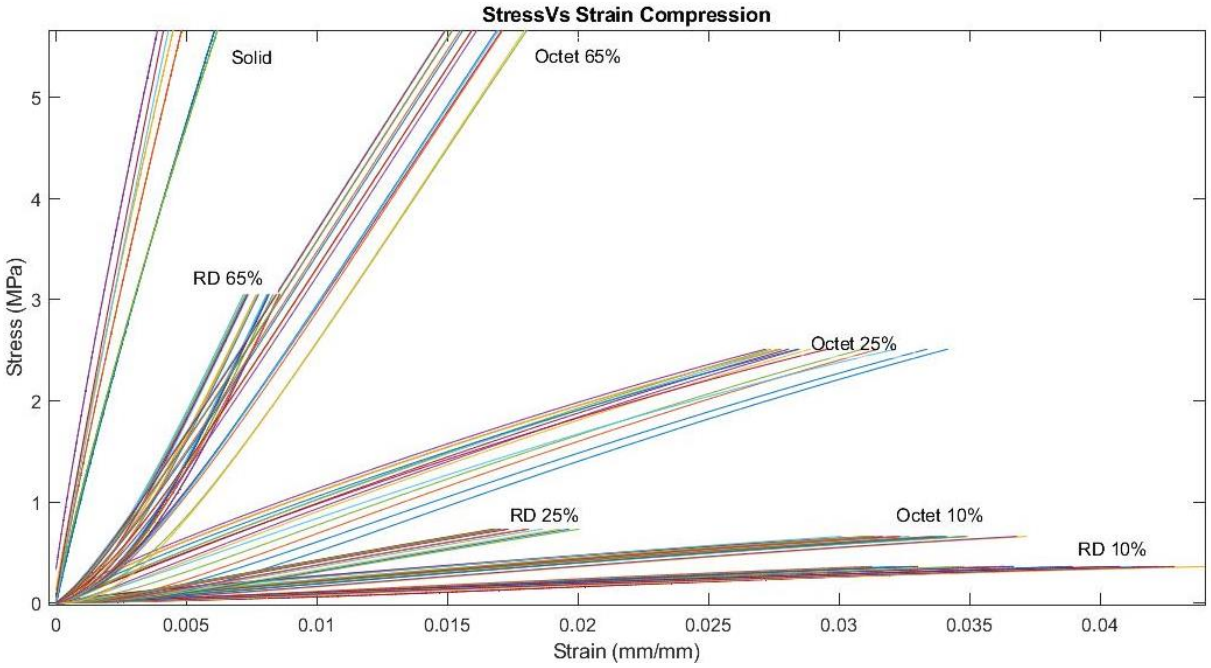

Figure 4 shows a compilation plot of all of the compression test results. Each are grouped by their type and density.

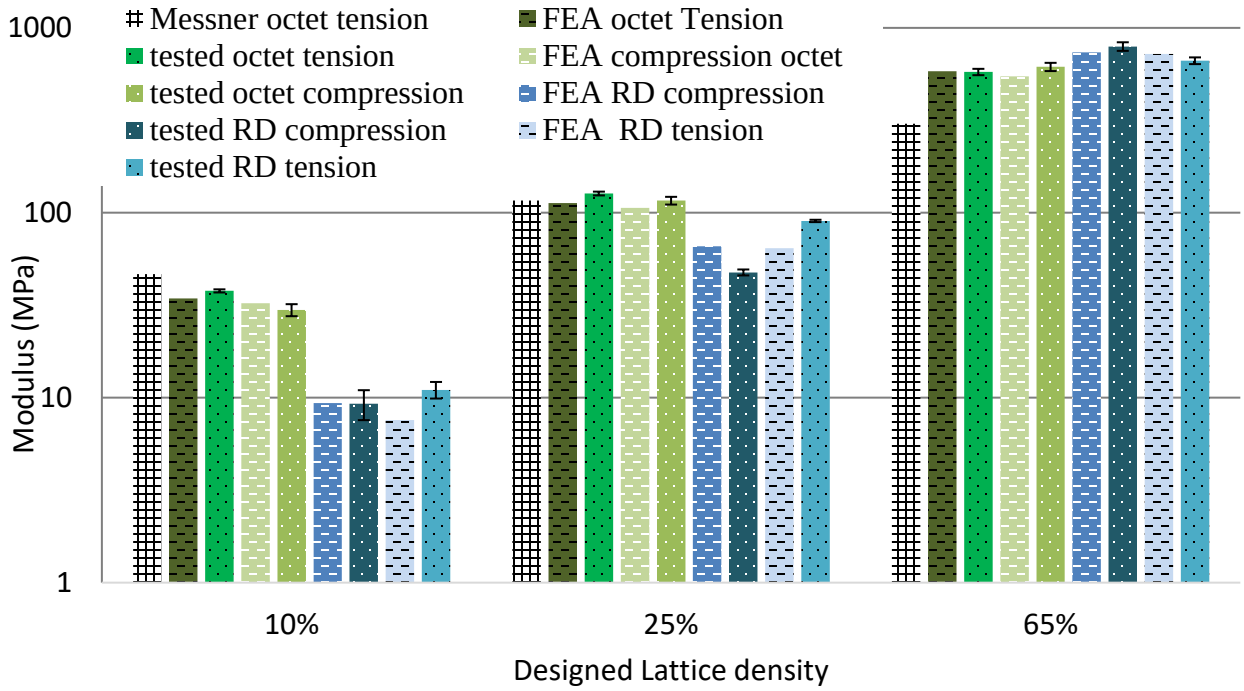

Figure 5 comparison of modulus values for all tests and predictive models (Messner preditions). The error bars are the standard deviation of the average tested modulus.

Discussion

As shown in Figure 3, the elastic modulus of the tensile samples varied greatly depending on the type of lattice and density. The curves of moduli seem to indicate the possibility of predicting a general modulus for a new density or lattice type from known data. Figure 3 also shows that the rhombic dodecahedron (RD) samples were consistently more compliant than the Octet samples, below the highest lattice density tested. This change in stiffness relative to the Octet could be due to the material at the node preventing the module from bending. The prevention of movement and the possible over cure of material could mean that the RD samples are more sensitive to density changes due to over cure than the Octet samples. The 25 Octet samples in Figure 3 also show a larger spread in moduli. This spread doesn't appear to be linked with the density uncertainty as shown in the averages in Table 1. The largest spread of tests in Figure 3 is that of the solid revealing a modulus between 2800 and 3300 MPa. It is also worth noting that both the RD and Octet 65 samples are stiffer than the solid material. The larger spread in the moduli lines in Figure 4 might be due to over curing; however, as with the spread in Figure 3, the density measurements do not support an exact correlation. The RD samples are also less stiff in Figure 4 than the Octet samples at the lower densities. The stiffness of the solid sample in compression as shown in Figure 4 shows that the material is much stiffer in compression than tension.

Comparing the bars in the Figure 5 show that the predicted modulus from the FEA modeling was similar in value to those measured in testing, with a max of 13% error for the octet and max of 46% error for the rhombic dodecahedron. Figure 5 also shows the high inaccuracy of the Messner equations when used to predict the modulus in octet samples. The differences between the Messner predictions are small at lighter densities, ~6% for 10 dense the error increases as the density increases until there is 147% error in compression for the 65 octet sample. Comparing the tested moduli of the tension and compression samples shows they are within 18% difference for Octet. However, the RD compression values increase more dramatically than the tension values as the density increases meaning the compressive modulus for RD is higher than the tension modulus. The octet 25 and 65 dense have negligible difference in moduli with an error less than 10%; however, the 10 dense octet has a 29% difference in moduli between the compression and tension tests. The rhombic dodecahedron samples at 10 and 65 are similar with a ~20% difference between compression and tension values, but the 25 dense is dramatically different with a 90% difference between the compression and tension moduli. This dramatic difference between compression and tension moduli for the 25 dense rhombic dodecahedron sample shows its dependence on stretch dominated movement. In compression the sample is not able to stretch as far compared to when the sample is in tension. Further study into this movement is required as it was only visible in the 25 sample due to the possible over curing evident in the 65 dense sample and the greater nodal flexibility due to less material in the 10 dense sample.

Future Studies

Testing geometrically different lattice types and densities would improve our understanding of the mechanical responses of printed lattices. Additionally, looking at yield strengths by continuing mechanical testing through yield and investigating the modulus graphs for 25% Octet graphs

would also be beneficial in our mechanical understanding of rhombic dodecahedron and octet lattices. Determining why the 65% samples are stiffer than the solid material by testing other densities and mapping the stress strain of the lattice would also help broaden understanding of our lattice properties. Finally, printing lattices out of other materials would assist in broadening the availability of materials for the design goals of this and future projects.

Conclusion

The mechanical characterization of the elastic moduli of printed octet and rhombic dodecahedron lattices in tension and compression showed the structural properties of a stereolithographically 3D printed lattice could be predicted using modeling within 13% in the octet and 46% in the rhombic dodecahedron. The FEA modeling matched closely to the elastic modulus determined through testing. This data will be used to provide accurate values for material properties required for topology optimization modeling. The uncertainties related to additively manufactured lattices were determined to be within ~7%, which allows for better situational design decision making regarding the lattice type and design density best suited for the project. Specifically, over curing explained why the 65% dense lattices had noticeably different moduli compared to the as-designed and FEA predations. It was also determined that the Messner predictions were increasingly incorrect at higher densities.

References

1. Maconachie, T., et al., *SLM lattice structures: Properties, performance, applications and challenges.* Materials & Design, 2019. **183**: p. 108137.
2. Bagheri,A., et al., *Determination of the Elasticity Modulus of 3D-Printed Octet-Truss Structures for Use in Porous Prosthesis Implants.* 2018. **11**: p. 2420.
3. Azzouz, L., et al., *Mechanical properties of 3-D printed truss-like lattice biopolymer non-stochastic structures for sandwich panels with natural fibre composite skins.* Composite Structures, 2019. **213**: p. 220-230.
4. Song, J., et al., *Octet-truss cellular materials for improved mechanical properties and specific energy absorption.* Materials & Design, 2019. **173**: p. 107773.
5. Vannutelli, R., *Mechanical behavior of 3d printed lattice structured materials.* 2017.
6. Bernardin, et al., *Topology Optimization, Additive Manufacturing, and Embedded Sensing Capabilities to Support the Development of High Fidelity Mechanical Mocks,LA-CP-20-20763, Los Alamos National Laboratory, 2020.*
7. Messner, M.C., et.al., *Wave propagation in equivalent continuums representing truss lattice materials.* International Journal of Solids and Structures, 2015. **73-74**: p. 55-56.
8. Messner, M.C., *Optimal lattice-structured materials.* Journal of the Mechanics and Physics of Solids, 2016. **96**: p. 162-183.
9. Pasvanti, N., et al., *LATTICE STRUCTURES MODELING:INTRODUCTION TO HOMOGENIZATION*, in *Before Reality Conference*. 2019: Munich, Germany
10. Martinez, E., et.al., *Characterizing Mechanical Behaviors in Varying Relatively Dense AM Lattice Structures Using FEA. Los Alamos National Laboratory,* 2021.

Appendix A: Stress-Strain Curves

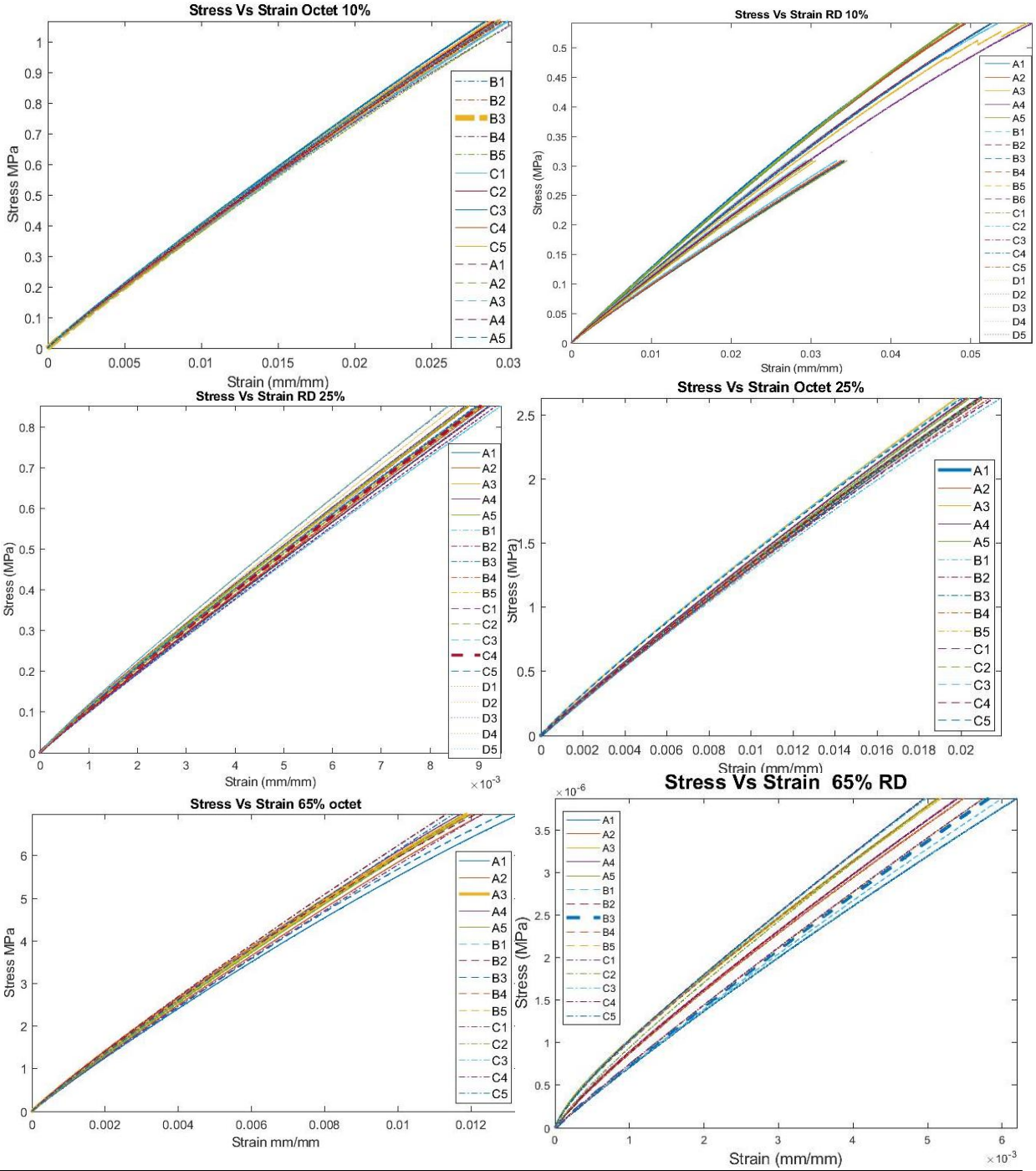

Tension Test data for all samples separated by the density and type of sample. The average curve is bolded.

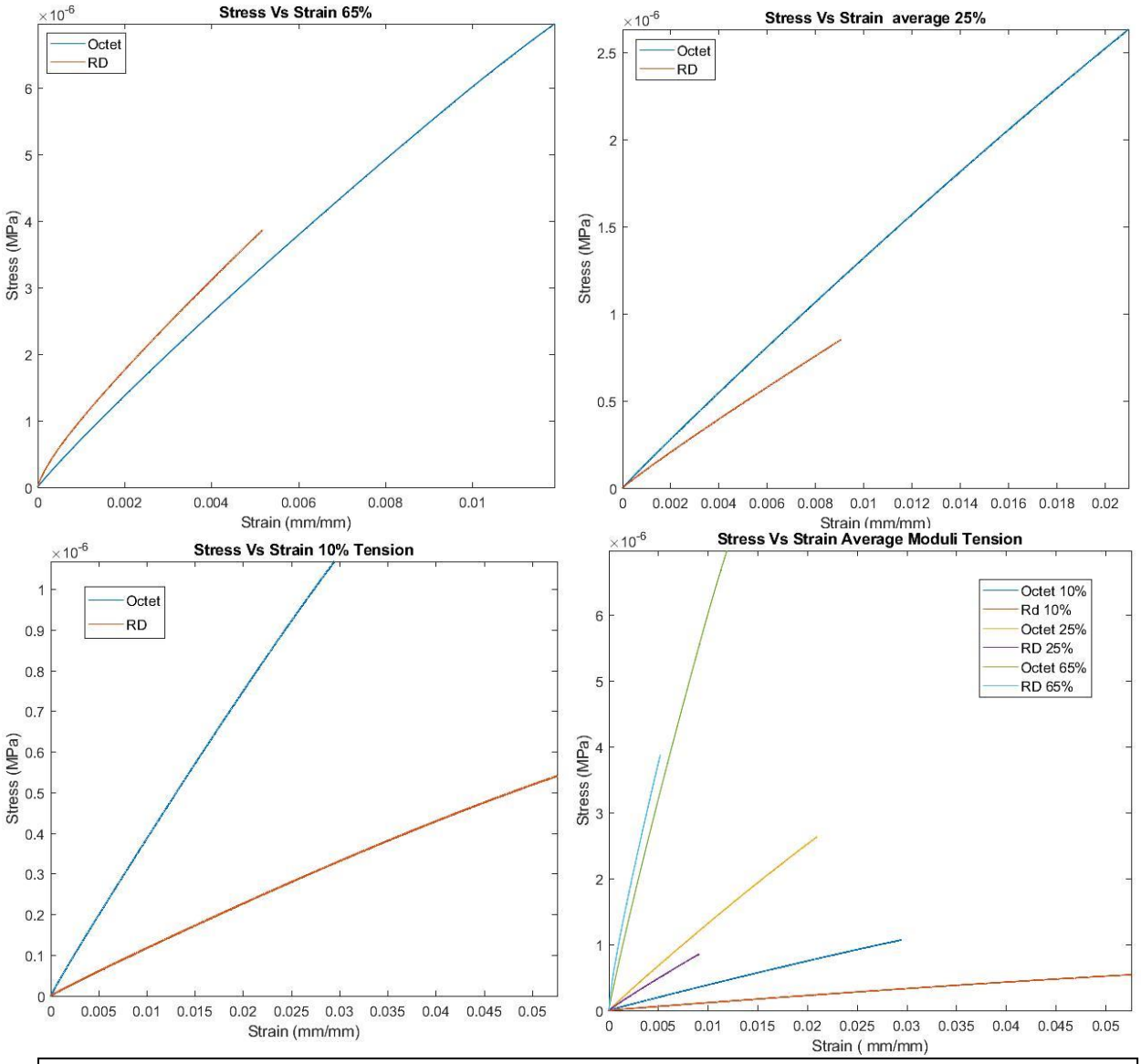

Average tensile curves for rhombic dodecahedron and Octet samples Graphs against each other separated by density. Final graph shows all average curves on the same plot.

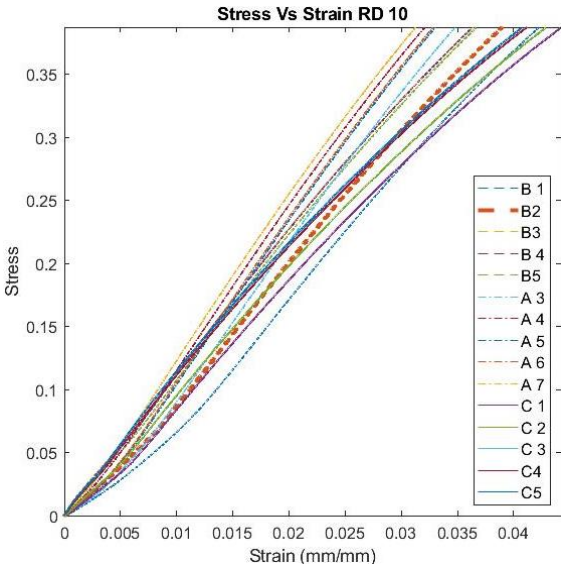

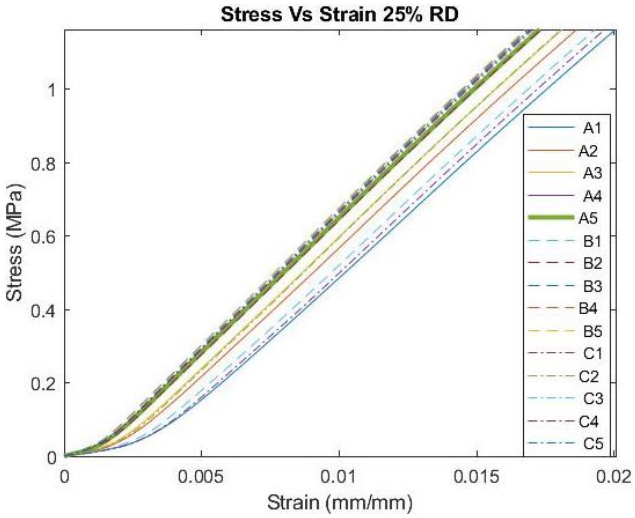

Compression Test data for the Rhombic dodecahedron separated by the density of the sample. The average curve is bolded.

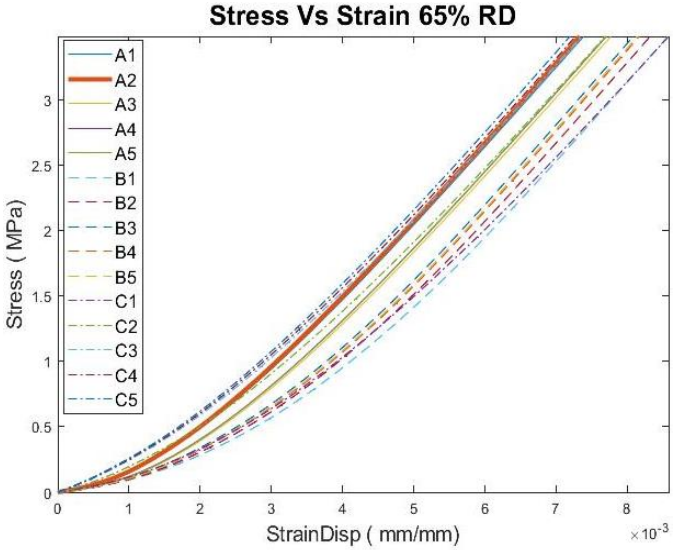

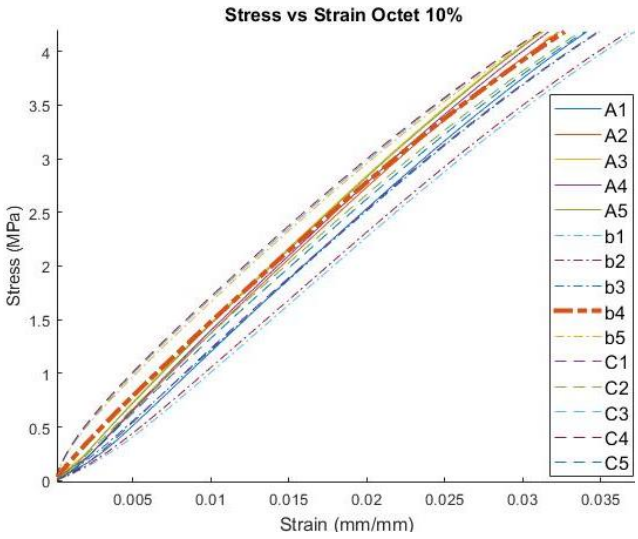

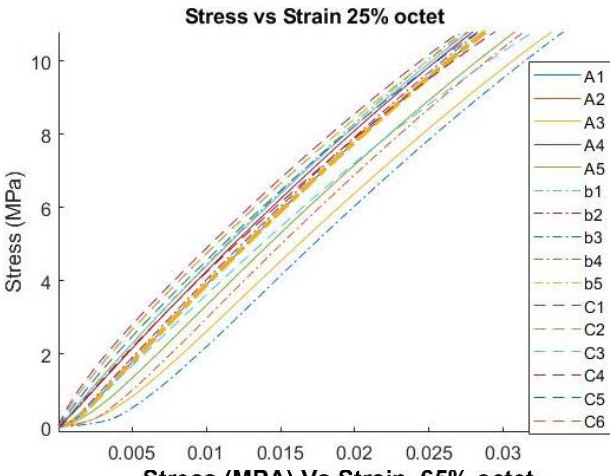

Compression test data for Octet samples separated by density of the sample. The average curve is bolded.

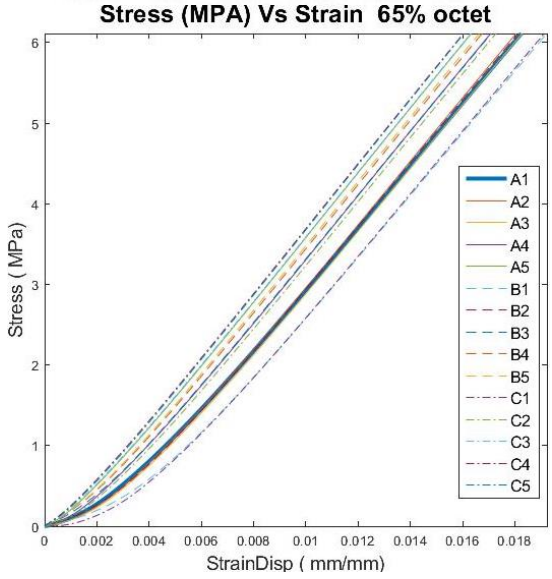

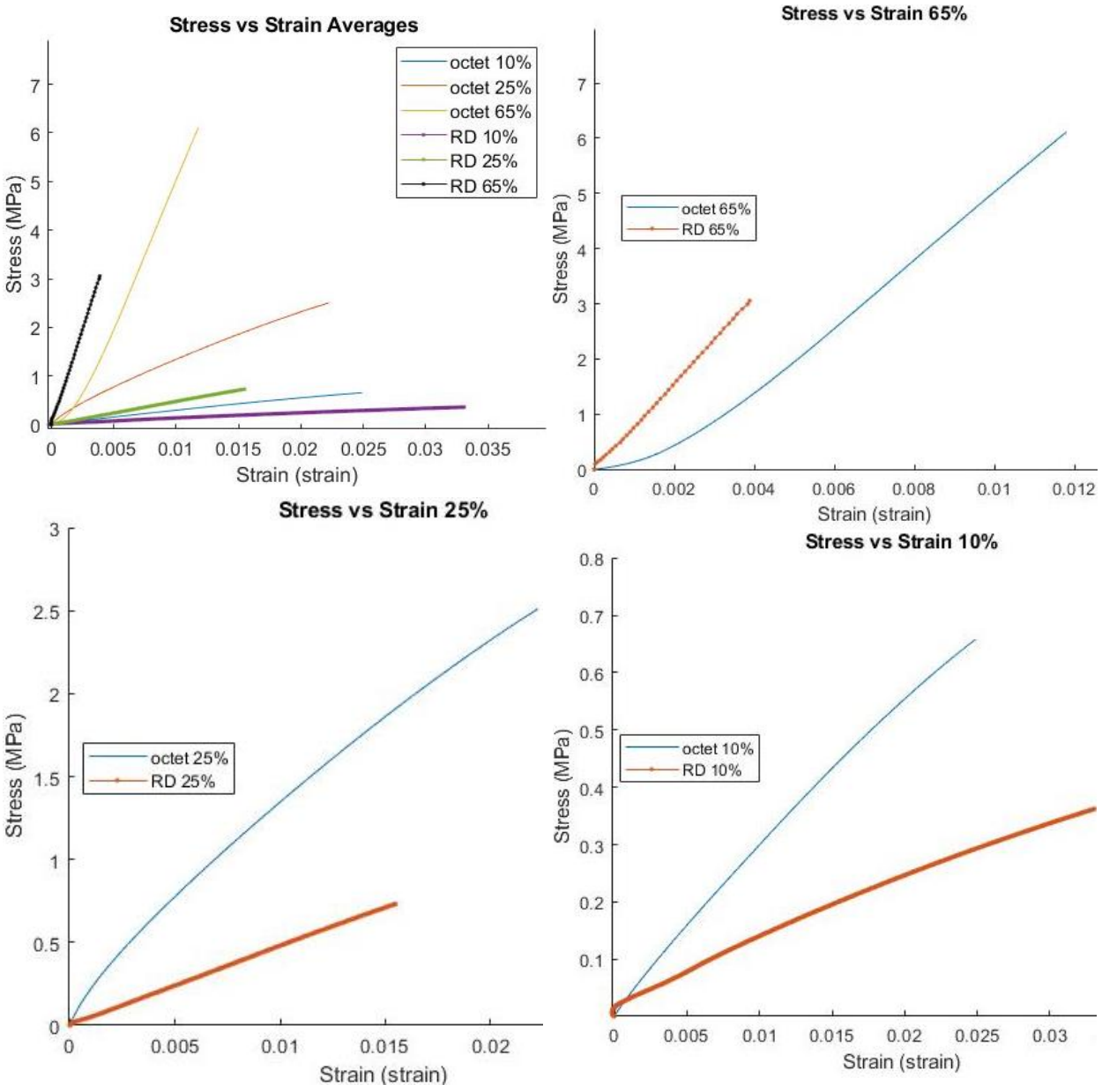

Average compression curve separated by density. First graph shows all averaged curves together.

Appendix B: Tabulated Data

Table Showing the moduli for each compression test in MPa						
Sample name	Octet 10%	Octet 25%	Octet 65%	RD 10%	RD25%	RD65%
A1	28.6524	109.4394	615.6899	10.8785	44.115	800.2263
A2	30.2213		637.3737	11.5581	45.3545	796.574
A3	32.3832	113.9802	635.322	11.6563	46.2442	788.5532
A4	31.2612	121.8023	653.2661	11.6317	47.4842	785.4238
A5	31.9695	121.1727	677.5476	11.5274	47.5552	781.1891
A6	34.0316					
B1	26.0947	109.1039	559.958	8.95909	45.2938	823.8507
B2	26.1375	115.0683	573.8253	8.96645	47.8444	844.5889
B3	27.1609	120.8711	588.62	8.75304	48.6198	852.2026
B4	29.8041	123.3636	598.7519	8.80707	48.6503	846.7436
B5	30.5847	126.0761	602.8617	8.89136	48.9578	849.8181
C1	28.372	107.2264	581.7867	7.75576	46.5491	725.2478
C2	29.1933	116.9295	617.5126	7.59918	48.5038	737.1595
C3	31.1769	112.6658	627.0612	7.36534	49.4918	751.7355
C4	31.1846	113.06	631.1216	7.3898	49.7034	755.8242
C5	29.0105	118.9453	633.2592	7.37168	49.8619	764.3066
C6		116.1896				
mean	29.8274	116.3929	615.59717	9.274051	47.61528	793.5629
Standard deviation	2.228168	5.602563	31.583929	1.708281	1.761559	42.36604
range	7.9369	18.8497	117.5896	4.29096	5.7469	126.9548

Table showing the moduli for each tension test in MPa						
Sample name	Octet 10%	Octet 25%	Octet 65%	RD 10%	RD25%	RD65%
A1	36.5749	127.2264	531.245	12.2255	90.2468	648.8809
A2	36.5807	130.3101	566.9482	11.9856	91.0637	690.5533
A3	37.4801	131.6716	577.0969	12.0103	92.2765	696.7862
A4	37.1589	130.571	580.5427	12.1896	92.5455	699.1208
A5	37.4646	129.9533	575.723	11.9373	92.5063	699.7693
B1	37.4424	121.5109	554.5789	11.2191	87.844	598.2438
B2	38.2392	125.3358	570.7703	11.1401	89.2812	652.2248
B3	37.675	126.173	554.1697	11.0507	89.9793	665.1544
B4	38.3829	124.0462	572.5641	12.6717	90.1397	662.4372
B5	38.5807	125.4772	574.7889	10.6059	90.0365	668.9822
C1	37.6067	123.0152	574.5908	9.55642	88.6685	628.3906
C2	38.5203	126.6025	598.4702	10.3748	89.9057	670.0565
C3	38.9345	129.3743	611.3121	9.61579	90.2016	650.6789

C4	38.1323	126.7415	613.3375	9.20244	90.2645	680.8138
C5	38.583	129.2057	609.4429	9.72739	90.5372	658.7267
Mean	37.824	127.148	577.705	11.034	90.366	664.721
Standard deviation	0.730	2.991	22.844	1.135	1.323	27.771
Range	2.360	10.161	82.093	3.469	4.702	101.526

Table showing the average moduli for each test as well as those from predictions.

Multicell Tension						
Unit Cell	Designed Density	E, predicted Messner (MPa)	E, FEA LANL (MPa)	E, Experimental (MPa)	Standard deviation	Range
Octet	10%	46.7	34.36	37.82	0.73	2.36
Octet	25%	116.7	112.89	127.15	2.99	10.16
Octet	65%	303.3	581.73	577.71	22.84	82.09
R D	10%	N/A	7.58	11.03	1.14	3.47
R D	25%	N/A	64.28	90.37	1.32	4.70
R D	65%	N/A	721.32	664.72	27.77	101.53
MultiCell Compression						
Octet	10%	38.33	32.44	29.83	2.23	7.94
Octet	25%	95.83	106.39	116.39	5.60	18.85
Octet	65%	249.17	545.85	615.60	31.58	117.59
R D	10%	N/A	9.34	9.27	1.71	4.29
R D	25%	N/A	65.86	47.62	1.76	5.75
R D	65%	N/A	738.40	793.56	42.37	126.95